Bulletin of the Seismological Society of America, Vol. 99, No. 3, pp. 2012–2019, June 2009, doi: 10.1785/0120080069

Short Note

Is There a Basis for Preferring Characteristic Earthquakes over a Gutenberg–Richter Distribution in Probabilistic Earthquake Forecasting?

by Tom Parsons and Eric L. Geist

Abstract The idea that faults rupture in repeated, characteristic earthquakes is central to most probabilistic earthquake forecasts. The concept is elegant in its simplicity, and if the same event has repeated itself multiple times in the past, we might anticipate the next. In practice however, assembling a fault-segmented characteristic earthquake rupture model can grow into a complex task laden with unquantified uncertainty. We weigh the evidence that supports characteristic earthquakes against a potentially simpler model made from extrapolation of a Gutenberg–Richter magnitude-frequency law to individual fault zones. We find that the Gutenberg–Richter model satisfies key data constraints used for earthquake forecasting equally well as a characteristic model. Therefore, judicious use of instrumental and historical earthquake catalogs enables large-earthquake-rate calculations with quantifiable uncertainty that should get at least equal weighting in probabilistic forecasting.

Introduction

Should we expect large ($M \sim 7$ and greater) earthquakes to behave differently than small ones? Probabilistic earthquake forecasting is commonly driven by the idea that large, characteristic earthquakes repeatedly rupture the same fault segments with the same magnitude and slip distribution, departing from the expected magnitude-frequency trend of smaller events. The characteristic model is derived from paleoseismic observations (Schwartz and Coppersmith, 1984; Wesnousky, 1994; Hecker and Abrahamson, 2004) and has great appeal for forecasting because if the same event has occurred repeatedly in the past, there is implied predictability. For the last ~20 yr, global earthquake forecasts have employed characteristic earthquake models to calculate expected rupture rates (e.g., McCann *et al.*, 1979; Working Group on California Earthquake Probabilities [WGCEP], 1988, 1990; Nishenko, 1991; WGCEP, 1995; Frankel *et al.*, 2002; WGCEP, 2003; Parsons, 2004; Earthquake Research Committee, 2005; Romeo, 2005; Petersen *et al.*, 2008; WGCEP, 2008).

By definition, characteristic earthquakes on individual faults are not subject to magnitude-frequency laws (Ishimoto and Iida, 1939; Gutenberg and Richter, 1954) wherein earthquakes are observed to obey a linear power-law distribution as $\log(N_M) = a - bM$, where a and b are constants, and N is the number of earthquakes greater than magnitude M. That distribution is commonly referred to as Gutenberg–Richter behavior. For very large regions, there is no dispute that earthquakes of all magnitudes scale according to the linear power law. Gutenberg–Richter behavior is also observed for subregions and individual faults for the most frequent lower-magnitude earthquakes (e.g., Abercrombie and Brune, 1994; Westerhaus *et al.*, 2002; Schorlemmer *et al.*, 2003, 2004; Wyss *et al.*, 2004; Parsons, 2007). However, because characteristic earthquakes on a given fault are thought to always be about the same size, their rates are proposed to be higher than expected from extrapolation of a linear Gutenberg–Richter relation (Fig. 1) (e.g., Schwartz and Coppersmith, 1984; Wesnousky, 1994; Hecker and Abrahamson, 2004; c.f., Kagan, 1996).

Implications of a chosen earthquake distribution model on earthquake probability calculations are critical. For a characteristic model, much effort is exerted on seeking out earthquake return times of infrequent, specific large-magnitude events that are expected to represent almost all the hazard. With the characteristic model, it is difficult to quantify uncertainties surrounding fault segmentation, characteristic magnitude assignment, and rupture boundaries (e.g., Savage, 1991, 1992; Page and Carlson, 2006). Often, these uncertainties are omitted (e.g., WGCEP, 2008). If instead a linear Gutenberg–Richter model applies to individual faults, then rates of the largest events are directly extrapolated from observation of smaller, instrumentally recorded earthquakes. A further implication of a Gutenberg–Richter model is that ruptures can occur over a broader magnitude range.

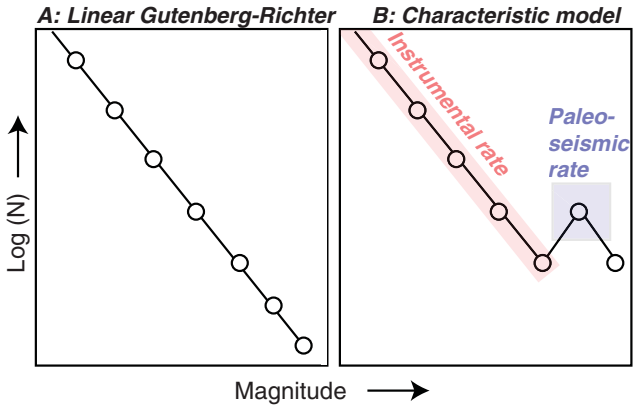

Figure 1. (a) Sketch of typical linear Gutenberg–Richter magnitude-frequency relation. In (b), there is a bump where higher-rate characteristic large-magnitude earthquakes are proposed.

It is not uncommon for aspects of Gutenberg–Richter and characteristic behavior to be incorporated in probabilistic forecasting, although there is typically a strong preference toward use of the characteristic model for major faults (e.g., type A faults, which typically have available paleoseismic data and highest slip rates [WGCEP, 1995]). As an example, characteristic rupture models got 90% weighting for sources of the largest possible earthquakes in the WGCEP (2008) forecast. The fit of both characteristic and Gutenberg–Richter rupture models to observations is examined here because probability and shaking hazard calculations are so strongly affected by model choice.

Earthquake Distribution Model and Data Constraints

Key data that inform earthquake rate forecasts are geologic and geodetic estimates of long-term fault slip rates and paleoseismic event rates and magnitudes, as well as instrumental/historical earthquake catalogs. As of this writing, official forecasts in the United States do not yet embrace physics-based models because of the added number of free parameters (e.g., Petersen *et al.*, 2008; WGCEP, 2008). Instead, the preferred method has been to derive rupture models from the aforementioned empirical constraints. By definition, a characteristic earthquake model readily fits the empirical data because (1) in the model, virtually all fault slip is caused by repeated characteristic events that mimic the long-term slip distribution, (2) the model is derived from paleoseismic observations in the first place, and (3) if a large enough region is considered, it can be fit to a regional Gutenberg–Richter distribution, although this can be a challenge (c.f., WGCEP, 2008). Less certain is whether a model with linear Gutenberg–Richter behavior occurring on individual faults can meet these observed data constraints.

We developed an algorithm to invert for long-term earthquake distribution on theoretical faults to assess the use of a Gutenberg–Richter model. Constraints were geologic slip rate and a fixed number of earthquakes (magnitude range M 5.0–7.8) obeying a linear Gutenberg–Richter distribution with b-value (slope) of 1.0. Our example model had two branching strike-slip fault surfaces 700 and 500 km long, discretized into 2.5 by 2.5 km patches that slipped at 40 and 20 mm/yr, respectively, for 1000 yr (Fig. 2). Model duration, slip rates, and rake are trade-offs that only matter in terms of establishing seismic moment balance in the model.

Initial earthquake nucleation sites were assigned randomly, and magnitudes were sampled from the Gutenberg–Richter distribution. Rupture areas were assigned from the empirical magnitude-area relation of Hanks and Bakun (2008). Event slip was calculated through the moment-magnitude relation of Hanks and Kanamori (1979) assuming a shear rigidity of $\mu = 3 \times 10^{10}$ N m. Contiguous, uniform-slip ruptures were initially allowed to grow at random into adjoining patches until they covered their magnitude-appropriate areas. Iterations were updated by assigning slip of a growing rupture preferentially to patches with the smallest prior accumulated slip, with the assumption that lowest prior slip implies highest failure stress. As the model was updated, if a randomly assigned hypocenter landed in a patch that produced cumulative slip in excess of the cumulative long-term slip constraint (plus 10% uncertainty), that event was repeatedly moved to new locations at random until its slip could be accommodated. Ruptures were allowed to jump between fault branches within a 4 km distance (Barka and Kandinsky-Cade, 1988; Harris, 1992; Harris and Day, 1993, 1999; Lettis *et al.*, 2002), with the decision governed by preexisting slip distribution (low slip equals high stress); modeled dynamic rupture jumps are shown to be most encouraged by a high stress state (e.g., Harris and Day, 1993, 1999). Figure 2b shows that a Gutenberg–Richter model was able to fit observed geologic slip rates within ± 3 mm/yr. Calculated event rates for $M \geq 6.7$ earthquakes averaged about 7.5 ± 2 per 1000 yr on the two segments, similar to the observed average rate of 6 ± 2 observable events per 1000 yr on comparable southern San Andreas fault segments, which have long records (~300–1500 yr) and slightly slower slip rates (~20–35 mm/yr) than the model faults (Biasi *et al.*, 2002; Fumal, Rymer, and Seitz, 2002; Fumal, Weldon, *et al.*, 2002).

Examination of Characteristic Earthquake Model Constraints

Two primary arguments are made in support of the characteristic earthquake model: (1) where repeated paleoearthquake offsets are measured, they are relatively uniform, and (2) paleoseismic event rates are higher than expected from extrapolation of a linear Gutenberg–Richter slope using smaller earthquakes recorded on or near a fault (Schwartz and Coppersmith, 1984; Wesnousky, 1994) (Fig. 1). We examine each of these arguments with respect to a simulated

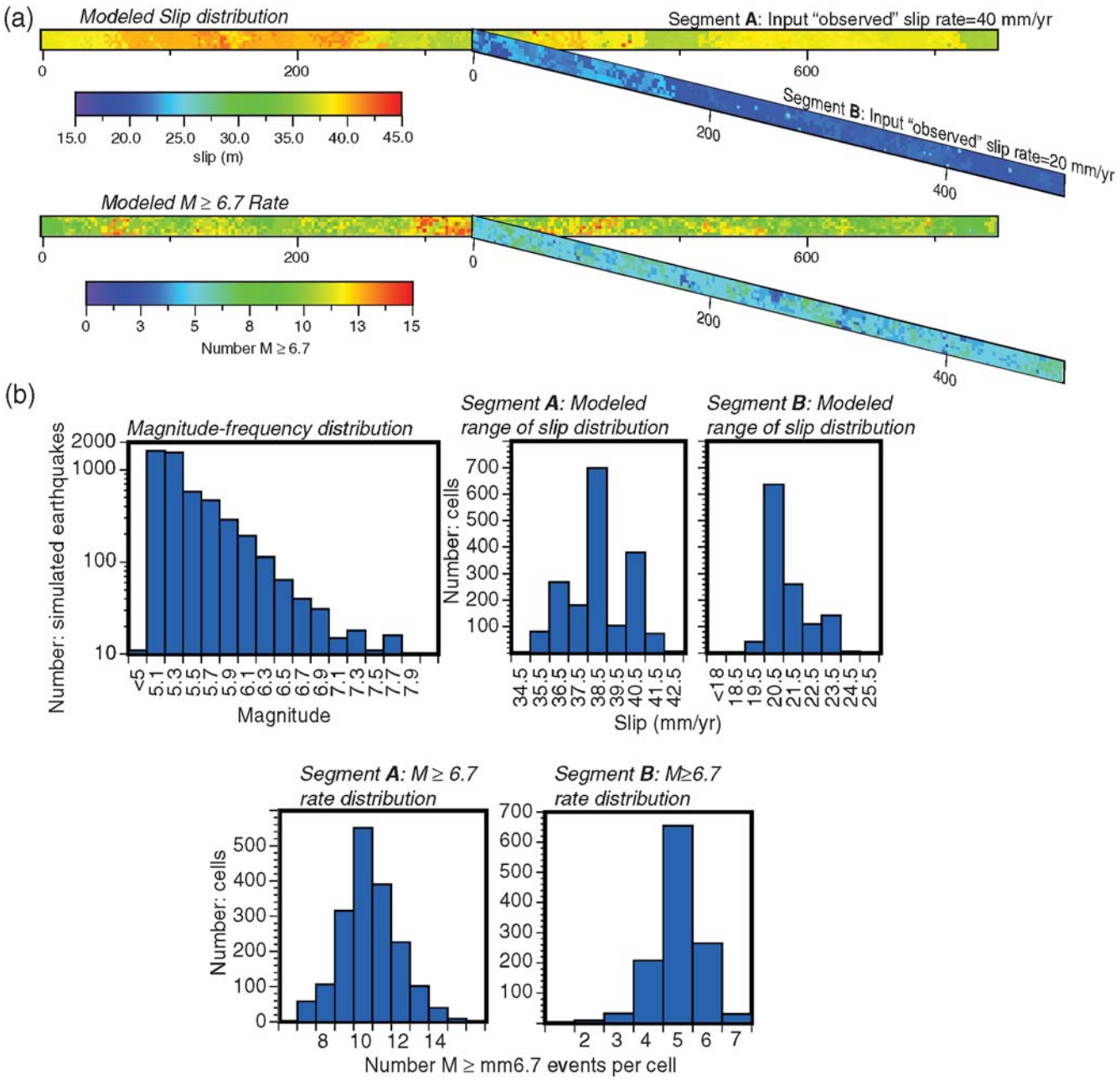

Figure 2. (a) Perspective view of the model fault configuration, contoured slip, and event-rate ($M \geq 6.7$) participation for a Gutenberg–Richter distribution on faults. (b) Histograms with the magnitude-frequency distribution as well as variation of model slip and events on 2.5 by 2.5 km patches.

earthquake catalog built from the Gutenberg–Richter model shown in Figure 2.

Event-Slip Observations

The characteristic earthquake model was born from recognizing repeated, very similar fault offsets in the geological record, particularly along the Wasatch fault zone in Utah, and the San Andreas fault in southern California (Schwartz and Coppersmith, 1984) and reinforced globally (Hecker and Abrahamson, 2004). Plotted in Figure 3 (blue line and error bars) are observed individual offsets and uncertainty for the Wasatch segments (Chang and Smith, 2002) and the south San Andreas fault site of Wrightwood (Weldon *et al.*, 2004). The issue is complicated on the San Andreas fault because the best event-slip measurements available are from the Wrightwood site, which lies at an assigned segment boundary (WGCEP, 2008) and may thus see ruptures from two different characteristic segments, although the distribution of event slip is not bimodal (Fig. 3a). Dip-slip offsets such as those along the Wasatch front are easier to measure

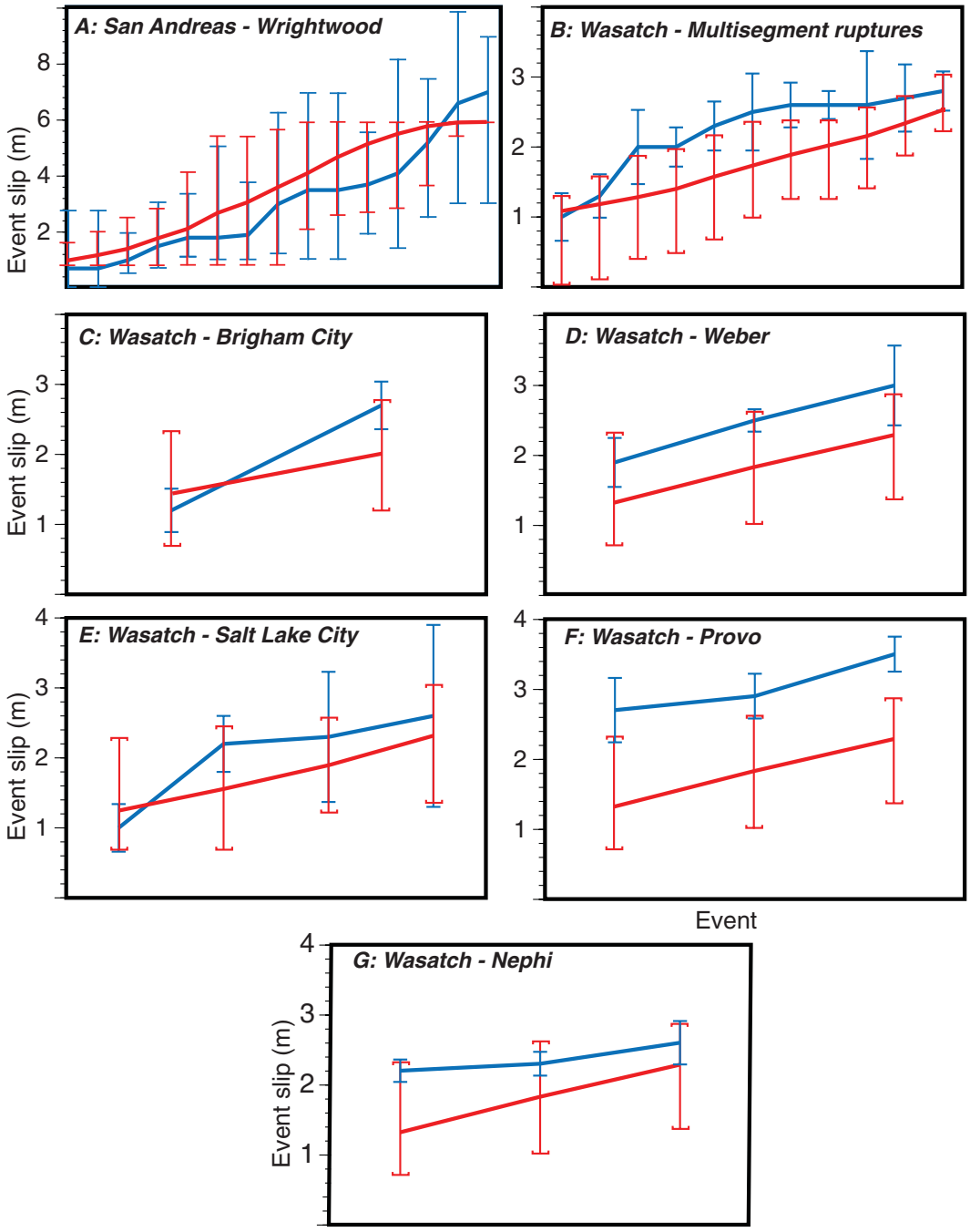

Figure 3. Observed individual event slip from paleoearthquakes at (a) Wrightwood on the San Andreas fault (Weldon *et al.*, 2004), and (b–g) Wasatch fault segments (Chang and Smith, 2002). Blue lines show observed slip values in meters, blue error bars indicate measurement uncertainty, and values are sorted from smallest to largest. Red lines show means of slip drawn from the Gutenberg–Richter model of Figure 2, with red error bars showing 95% of the range of 50 random draws. We assumed, based on the observations, that the minimum threshold of observation is ~0.7 m (M ~6.6) on the San Andreas fault and ~1.0 m (M ~6.8) on the Wasatch. (b) Mean slip values from the Wasatch multisegment model of Chang and Smith (2002); (c–g) slip values if ruptures are confined to single segments.

in the paleoseismic record than strike-slip ruptures because they leave visible fault scarps.

To test a Gutenberg–Richter model against event-slip observations, we made repeated random draws of slip events from surface points of the model depicted in Figure 2 to simulate each of the sites plotted in Figure 3. Because the model in Figure 2 is slip balanced, the time, rake, and slip-rate factors cancel each other out, and we can use the model to compare the spatial distribution of earthquake ruptures to any real fault site up to its maximum expected magnitude threshold. We can thus use the Gutenberg–Richter distribution of event slip drawn from the moment-balanced

model for comparison with both the San Andreas and Wasatch fault observations. We assumed, based on the observations plotted in Figure 3, that 0.7 m offsets ($M \sim 6.6$) represent the smallest resolvable paleoslip on the San Andreas fault and 1.0 m offsets ($M \sim 6.8$) are resolvable on the Wasatch fault. Given the nature of power-law magnitude-frequency distributions, the most likely ruptures to have occurred in the model at a given site are the smallest ones (Fig. 2b). Therefore, limited sampling (i.e., the 2–15 events of Fig. 3) yields a series of individual slip events that have almost the same offset.

When we randomly draw 50 sets of 2–15 synthetic ruptures from the Gutenberg–Richter model of Figure 2, we are able to reproduce observations of Figure 3 (red error bars) within reported uncertainties (blue error bars) with the exception of the Provo single-segment event-slip model (Fig. 3f) on the Wasatch fault. Observations that are matched by a Gutenberg–Richter model include San Andreas fault offsets at Wrightwood (Weldon *et al.*, 2004) (Fig. 3a), the Wasatch fault multisegment rupture models of Chang and Smith (2002) (Fig. 3b), and all but one of the Wasatch single-segment rupture models. We conclude from this that a Gutenberg–Richter model should not be excluded based on observation of similar rupture offsets.

Instrumental versus Paleoseismic Magnitude-Frequency Trends

For a broad region, magnitude-frequency resolution is such that a mixture of characteristic faults (e.g., Wesnousky, 1994; López-Ruiz *et al.*, 2004) or Gutenberg–Richter distributed faults with different maximum magnitude cutoffs (e.g., Kagan 2002a,b) can satisfy the linear power-law trend. The characteristic-versus-power-law issue hinges on more poorly resolved relations from individual fault zones. Arguments for the characteristic earthquake model are supported by calculations of higher paleoseismically determined earthquake rates than extrapolation of a power-law derived from earthquakes instrumentally recorded on and near individual faults (Schwartz and Coppersmith, 1984; Wesnousky, 1994) (e.g., Fig. 1b).

We plot magnitude-frequency distributions (see the Data and Resources section) in Figure 4a for a section of the southern San Andreas fault (identified in Fig. 4b), where there are numerous paleoseismic sites and abundant catalog seismicity. Comparisons between paleoseismic and instrumental magnitude-frequency behavior is very much dependent on both temporal and spatial sampling of the catalog and how paleoseismic rates are calculated (e.g., Stein and Newman, 2004; Stein *et al.*, 2005; Parsons, 2008). The paleoseismic rates we use for comparison in Figure 4 (from Biasi *et al.*, 2002; Fumal, Rymer, Seitz, 2002; Fumal, Weldon, *et al.*, 2002) were developed through uncertainty analysis by Biasi *et al.* (2002) and Parsons (2008) as used in the WGCEP (2008) earthquake rupture forecast, and the magnitude range is from the Weldon *et al.* (2004) event-slip data.

It is apparent that broader sampling of earthquake catalogs either temporally or spatially increases the overall rate. A very wide swath taken from 50 km on either side of the southern San Andreas fault from the ~1970–2007 catalog (see the Data and Resources section) produces a Gutenberg–Richter trend that is in accord with paleoseismic rates, whereas a ±5 km swath from the instrumental catalog projects lower rates. Sampling a ±5 km swath from a longer ~1850–2006 earthquake catalog (Felzer and Cao, 2008) (Fig. 4a) is also consistent with paleoseismic rates. The historic catalog has relatively few events, 20 $M > 4$ shocks were located within ±5 km of the San Andreas segment we investigated (Fig. 4b) and is subject to significant location uncertainty for the oldest events.

The instrumental catalog along the San Andreas fault may be influenced by the legacy of past large earthquakes (Harris and Simpson, 1996; Stein, 1999) or inherent rate fluctuations (Felzer and Brodsky, 2005). However, a narrow (±5 km) swath taken from a more active San Andreas fault segment in the Parkfield region is also consistent with southern San Andreas paleoseismic rates. The Parkfield segment did not participate (Harris and Simpson, 1996; Thatcher *et al.*, 1997) in either of California's largest historical earthquakes (the 1857 $M \sim 7.9$ Fort Tejon and the 1906 $M \sim 7.8$ San Francisco [e.g., Ellsworth, 1990] shocks), and thus might not be subject to stress shadowing effects if they have impacted seismicity rates (Harris and Simpson, 1996).

Attempting to reconcile paleoseismically determined event rates with Gutenberg–Richter relations projected with smaller, instrumental or historical earthquakes highlights the broader questions of what constitutes a fault zone, and how earthquakes interact with each other. If the analysis were restricted to the exact fault surface that ruptures during the largest earthquakes, it is clear that over instrumental catalog durations of a few decades, Gutenberg–Richter projections cannot match south San Andreas paleoseismic rates, implying support for a characteristic model (Fig. 1b). However, indications are that a longer (~150 yr) catalog from a implying narrow (±5 km) swath can also match the paleoseismic record (Fig. 4a).

Even the narrowest spatial definition (±5 km wide) of the San Andreas fault zone we consider incorporates minor subsidiary faults along with the main trace (Fig. 4b). It is clear that fault-zone definition, as well as earthquake catalog completeness and temporal rate fluctuations are important sources of uncertainty in applying a linear Gutenberg–Richter model to individual fault zones. However, in California and much of the rest of the world, the combined instrumental and historical catalogs are such that magnitude-frequency uncertainties are readily quantifiable (e.g., Felzer and Cao, 2008). In summary, examination of instrumental and historical earthquake catalogs shows that rates are dependent on space and time; thus completeness issues prevent us from identifying a clear basis for preferring either a char-

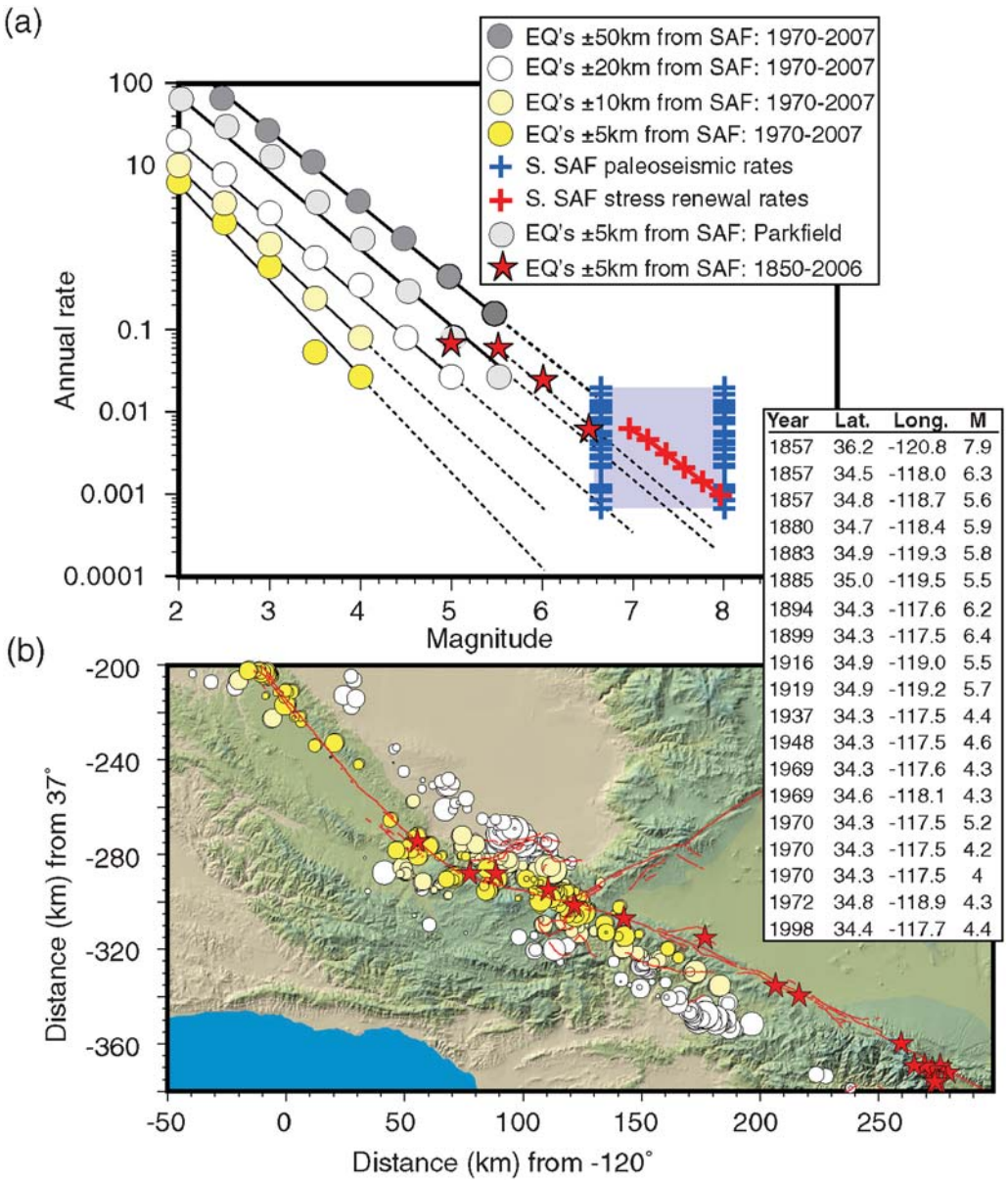

Figure 4. (a) Magnitude-frequency relations for a variety of earthquake catalogs, such as events taken from 5, 10, and 20 km of either side of the south San Andreas fault (epicenters shown in [b]). Also shown are relations for events taken from 50 km of either side of the fault trace, 5 km either side of a 100 km long section of the San Andreas from the more active Parkfield region and events taken from 5 km of either side of the south San Andreas fault from the 1850–2006 catalog of Felzer and Cao (2008) (red stars on [a] and [b]). Inset table gives individual historic event data. Blue + symbols show paleoseismic event rates for south San Andreas sites from Biasi *et al.* (2002) and Parsons (2008) and cover rate and magnitude uncertainties as applied by WGCEP (2008). Paleoseismic magnitudes are unknown, so rates are displayed between M 6.6 and M 8. Stress-renewal recurrence intervals for events between M 7 and M 8 from Parsons (2006) are shown by red + symbols.

acteristic earthquake model or a linear Gutenberg–Richter model on individual fault zones.

Conclusions

Probabilistic earthquake forecasts rely almost entirely on a small set of empirical data that the characteristic earthquake model readily matches. In probabilistic forecasts like the WGCEP (2008) effort, characteristic models get dominant weight for sources of the largest earthquakes. To determine if this tilt is justified, we compare the characteristic earthquake model with another empirical approach, a Gutenberg–Richter-distributed rupture model. We conclude that giving clear preference to either model in calculating future earthquake rates is not justifiable because a fault-based, linear Gutenberg–Richter distribution of earthquakes seems to match available data just as well as a characteristic model. The data we consider include the most-commonly used forecast constraints, such as long-term geologically and geodetically determined fault-slip rates, paleoseismic event

rates, individual event-slip observations, and subregional magnitude-frequency distributions. An important influence on using a linear Gutenberg–Richter model for extrapolating large earthquake rates is how a fault zone is defined in terms of which smaller earthquakes can be associated with it. However, rate uncertainties related to catalog selection are readily quantifiable and transferable to forecast uncertainty, which is in contrast with the often unwieldy and sometimes unquantifiable uncertainties associated with characteristic earthquake models.

Data and Resources

Earthquake catalogs used in this study to calculate magnitude-frequency distributions were acquired through the Advanced National Seismic System (ANSS) catalog search linked through the Northern California Earthquake Data Center (NCEDC) web site at http://www.ncedc.org/anss/catalog-search.html (last accessed April 2008).

Acknowledgments

We very much appreciate reviews by David Schwartz and Ivan Wong, both of whom prefer the characteristic earthquake model, but nonetheless supported publication of this alternative view, and provided many helpful comments that improved this discussion.

References

Abercrombie, R. E., and J. N. Brune (1994). Evidence for a constant b-value above magnitude 0 in the southern San Andreas, San Jacinto, and San Miguel fault zones, and at the Long Valley Caldera, California, *Geophys. Res. Lett.* **21,** 1647–1650.

Barka, A. A., and K. Kandinsky-Cade (1988). Strike-slip fault geometry in Turkey and its influence on earthquake activity, *Tectonics* **7,** 663–684.

Biasi, G. P., R. J. Weldon II, T. E. Fumal, and G. G. Seitz (2002). Paleoseismic event dating and the conditional probability of large earthquakes on the southern San Andreas fault, California, *Bull. Seismol. Soc. Am.* **92,** 2761–2781.

Chang, W.-L., and R. B. Smith (2002). Integrated seismic-hazard analysis of the Wasatch Front, Utah, *Bull. Seismol. Soc. Am.* **92,** 1904–1922.

Earthquake Research Committee (2005). Comprehensive study of probabilistic seismic hazard map for Japan, Headquarters for Earthquake Research Promotion, Tokyo, Japan, 125 pp.

Ellsworth, W. L. (1990). Earthquake history, 1769–1989, in *The San Andreas Fault System California*, R. E. Wallace (Editor), *U.S. Geol. Surv. Profess. Pap. 1515*, 153–187.

Felzer, K., and E. Brodsky (2005). Testing the stress shadow hypothesis, *J. Geophys. Res.* **110,** B05S09, doi 10.1029/2004JB003277.

Felzer, K., and T. Cao (2008). WGCEP historical California earthquake catalog, *U.S. Geol. Surv. Open-File Rept. 2007–1437-H*.

Frankel, A. D., M. D. Petersen, C. S. Mueller, K. M. Haller, R. L. Wheeler, E. V. Leyendecker, R. L. Wesson, S. C. Harmsen, C. H. Cramer, D. M. Perkins, and K. S. Rukstales (2002). Documentation for the 2002 update of the national seismic hazard maps, *U.S. Geol. Surv. Open-File Rept. OFR-02-420*, 33 pp.

Fumal, T. E., M. J. Rymer, and G. G. Seitz (2002). Timing of large earthquakes since A.D. 800 on the Mission Creek strand of the San Andreas fault zone at Thousand Palms Oasis, near Palm Springs, California, *Bull. Seismol. Soc. Am.* **92,** 2841–2860.

Fumal, T. E., R. J. Weldon II, G. P. Biasi, T. E. Daeson, G. G. Seitz, W. T. Frost, and D. P. Schwartz (2002). Evidence for large earthquakes on the San Andreas fault at the Wrightwood, California, Paleoseismic site: A.D. 500 to present, *Bull. Seismol. Soc. Am.* **92,** 2726–2760.

Gutenberg, B., and C. R. Richter (1954). Magnitude and energy of earthquakes, *Ann. Geof.* **9,** 1–15.

Hanks, T. C., and W. H. Bakun (2008). M-log A observations for recent large earthquakes, *Bull. Seismol. Soc. Am.* **98,** 490–494.

Hanks, T. C., and H. Kanamori (1979). A moment magnitude scale, *J. Geophys. Res.* **84,** 2348–2350.

Harris, R. A. (1992). Dynamic interaction of parallel strike-slip fault-segments: Some implications for the eastern San Francisco Bay area, in *Proc. of the 2nd Conf. on Earthquake Hazards in the Eastern San Francisco Bay Area*, G. Borchardt, S. E. Hirschfeld, J. J. Lienkaemper, P. McClellan and I. G. Wong (Editors), Calif. Div. Mines Geol. Spec. Publ., 113, 73–80.

Harris, R. A., and S. M. Day (1993). Dynamics of fault interaction: Parallel strike-slip faults, *J. Geophys. Res.* **98,** 4461–4472.

Harris, R. A., and S. M. Day (1999). Dynamic 3D simulations of earthquakes on en echelon faults, *Geophys. Res. Lett.* **26,** 2089–2092.

Harris, R. A., and R. W. Simpson (1996). In the shadow of 1857—the effect of the great Ft. Tejon earthquake on subsequent earthquakes in southern California, *Geophys. Res. Lett.* **23,** 229–232.

Hecker, S., and N. A. Abrahamson (2004). Low slip-at-a-point variability: Implications for earthquake-size distribution, fault rupture hazard, and ground-motion modeling: Basin and range seismic hazards summit II, Western States Seismic Policy Council, 16–19 May 2004, Program and Abstracts, 21–22.

Ishimoto, M., and K. Iida (1939). Observations sur les seismes enregistres par le microseimographe construit dernierement, *Bull. Earthq. Res. Inst. Univ. Tokyo* **17,** 443–478 (in Japanese with French abstract).

Kagan, Y. Y. (1996). Comment on "The Gutenberg–Richter or characteristic earthquake distribution, which is it?" by Steven G. Wesnousky, *Bull. Seismol. Soc. Am.* **86,** 274–285.

Kagan, Y. Y. (2002a). Seismic moment distribution revisited: I. Statistical results, *Geophys. J. Int.* **148,** 520–541.

Kagan, Y. Y. (2002b). Seismic moment distribution revisited: II. Moment conservation principle, *Geophys. J. Int.* **149,** 731–754.

Lettis, W., J. Bachhuber, R. Witter, C. Brankman, C. E. Randolph, A. Barka, W. D. Page, and A. Kaya (2002). Influence of releasing step-overs on surface fault rupture and fault segmentation: Examples from the 17 August 1999 Izmit earthquake on the North Anatolian fault, Turkey, *Bull. Seismol. Soc. Am.* **92,** 19–42.

López-Ruiz, R., M. Vázquez-Prada, J. B. Gómez, and A. F. Pacheco (2004). A model of characteristic earthquakes and its implications for regional seismicity, *Terra Nova* **16,** 116–120, doi 10.1111/j.1365-3121.2004.00538.x..

McCann, W. R., S. P. Nishenko, L. R. Sykes, and J. Krause (1979). Seismic gaps and plate tectonics: Seismic potential for major boundaries, *Pure Appl. Geophys.* **117,** 1082–1147.

Nishenko, S. P. (1991). Circum-Pacific seismic potential: 1989–1999, *Pure Appl. Geophys.* **135,** 169–259.

Page, M. T., and J. M. Carlson (2006). Methodologies for earthquake hazard assessment: Model uncertainty and the WGCEP-2002 forecast, *Bull. Seismol. Soc. Am.* **96,** 1624–1633, doi 10.1785/0120050195.

Parsons, T. (2004). Recalculated probability of $M \geq 7$ earthquakes beneath the Sea of Marmara, Turkey, *J. Geophys. Res.* **109,** B05304, doi 10.1029/2003JB002667.

Parsons, T. (2006). $M \geq 7.0$ earthquake recurrence on the San Andreas fault from a stress renewal model, *J. Geophys. Res.* **111,** B12305, doi 10.1029/2006JB004415.

Parsons, T. (2007). Forecast experiment: Do temporal and spatial b-value variations along the Calaveras fault portend $M \geq 4.0$ earthquakes?, *J. Geophys. Res.* **112,** B03308, doi 10.1029/2006JB004632.

Parsons, T. (2008). Monte Carlo method for determining earthquake recurrence parameters from short paleoseismic catalogs: Example calculations for California, *J. Geophys. Res.* **113,** B03302, doi 10.1029/2007JB004998.

Petersen, M. D., A. D. Frankel, S. C. Harmsen, C. S. Mueller, K. M. Haller, R. L. Wheeler, R. L. Wesson, Y. Zeng, O. S. Boyd, D. M. Perkins, N. Luco, E. H. Field, C. J. Wills, and K. S. Rukstales (2008). Documentation for the 2008 update of the United States national seismic hazard maps, *U.S. Geol. Surv. Open-File Rept. 2008-1128*, 61 pp.

Romeo, R. W. (2005). Earthquake hazard in Italy, 2001–2030, *Nat. Hazards* **36,** 383–405, doi 10.1007/s11069-005-1939-1.

Savage, J. C. (1991). Criticism of some forecasts of the National Earthquake Prediction Evaluation Council, *Bull. Seismol. Soc. Am.* **81,** 862–881.

Savage, J. C. (1992). The uncertainty in earthquake conditional probabilities, *Geophys. Res. Lett.* **19,** 709–712.

Schorlemmer, D., G. Neri, S. Weimer, and A. Mostaccio (2003). Stability and significance tests for *b*-value anomalies: example from the Tyrrhenian Sea, *Geophys. Res. Lett.* **30,** no. 16, 1835, doi 10.1029/2003GL017335.

Schorlemmer, D., S. Weimer, and M. Wyss (2004). Earthquake statistics at Parkfield: 1. Stationarity of b-values, *J. Geophys. Res.* **109,** B12307, doi 10.1029/2004JB003234.

Schwartz, D. P., and K. J. Coppersmith (1984). Fault behavior and characteristic earthquakes: Examples from the Wasatch and San Andreas fault zones, *J. Geophys. Res.* **89,** 5681–5698.

Stein, R. S. (1999). The role of stress transfer in earthquake occurrence, *Nature* **402,** 605–609.

Stein, S., and A. Newman (2004). Characteristic and uncharacteristic earthquakes as possible artifacts: Applications to the New Madrid and Wabash seismic zones, *Seism. Res. Lett.* **75,** 173–187.

Stein, S., A. Friedrich, and A. Newman (2005). Dependence of possible characteristic earthquakes on spatial sampling: Illustration for the Wasatch seismic zone, Utah, *Seism. Res. Lett.* **76,** 432–436.

Thatcher, W., G. Marshall, and M. Lisowski (1997). Resolution of fault slip along the 470-km-long rupture of the great 1906 San Francisco earthquake and its implications, *J. Geophys. Res.* **102,** 5353–5367.

Weldon, R., K. Scharer, T. Fumal, and G. Biasi (2004). Wrightwood and the earthquake cycle: What the long recurrence record tells us about how faults work, *GSA Today* **14,** 4–10, doi 10.1130/1052-5173(2004)014.

Wesnousky, S. G. (1994). The Gutenberg–Richter or characteristic earthquake distribution, which is it?, *Bull. Seismol. Soc. Am.* **84,** 1940–1959.

Westerhaus, M., M. Wyss, R. Yilmaz, and J. Zschau (2002). Correlating variations of *b* values and crustal deformation during the 1990s may have pinpointed the rupture initiation of the M_w 7.4 Izmit earthquake of 1999 August 17, *Geophys. J. Int.* **148,** 139–152.

Working Group on California Earthquake Probabilities (WGCEP) (1988). Probabilities of large earthquakes occurring in California on the San Andreas fault, *U.S. Geol. Surv. Open-File Rept.*, 62 pp.

Working Group on California Earthquake Probabilities (WGCEP) (1990). Probabilities of large earthquakes in the San Francisco Bay Region, California, *U.S. Geol. Surv. Circ.*, 51 pp.

Working Group on California Earthquake Probabilities (WGCEP) (1995). Seismic hazards in Southern California: probable earthquakes, 1994 to 2024, *Bull. Seismol. Soc. Am.* **85,** 379–439.

Working Group on California Earthquake Probabilities (WGCEP) (2003). Earthquake probabilities in the San Francisco Bay region: 2002 to 2031, *U.S. Geol. Surv. Open-File Rept. 03-214*.

Working Group on California Earthquake Probabilities (WGCEP) (2008). The uniform California earthquake rupture forecast, version 2 (UCERF 2), *U.S. Geol. Surv. Open-File Rept. 2007-1437*, California Geological Survey Special Report 203, 104 pp. (http://pubs.usgs.gov/of/2007/1437/).

Wyss, M., C. G. Sammis, R. M. Nadeau, and S. Weimer (2004). Fractal dimension and b-value on creeping and locked patches of the San Andreas fault near Parkfield, California, *Bull. Seismol. Soc. Am.* **94,** 410–421.

U.S. Geological Survey
MS-999, 345 Middlefield Road
Menlo Park, California, 94025

Manuscript received 15 May 2008